JACS
JOURNAL OF THE AMERICAN CHEMICAL SOCIETY

COMMUNICATION

pubs.acs.org/JACS

Anomalous Thermal Expansion in the Square-Net Compounds RE_4TGe$_8$ (RE = Yb, Gd; T = Cr−Ni, Ag)

Sebastian C. Peter,[†] Maria Chondroudi,[‡] Christos D. Malliakas,[†] Mahalingam Balasubramanian,[§] and Mercouri G. Kanatzidis*[,†,‡]

[†]Department of Chemistry, Northwestern University, 2145 Sheridan Road, Evanston, Illinois 60208, United States

[‡]Materials Science Division, Argonne National Laboratory, 9700 South Cass Avenue, Argonne, Illinois 60439, United States

[§]Advanced Photon Source, Argonne National Laboratory, Argonne, Illinois 60439, United States

Supporting Information

ABSTRACT: The family of materials RE_4TGe$_8$ (RE = Yb, Gd; T = transition metal) exhibits directional zero thermal expansion (ZTE) via a process that is associated with the linking of planar square nets in the third dimension. The Ge square nets in these compounds exhibit commensurate long-range modulations similar to those observed in charge-density-wave compounds. The ZTE is manifested in the plane of the square nets from 10 to 300 K with negligible volume expansion below ∼160 K. The specific atomic arrangement in RE_4TGe$_8$ enables a Poisson-like mechanism that allows the structure to contract along one direction as it expands only slightly in the perpendicular direction.

Substances generally undergo thermal expansion with increasing temperature, and materials with zero thermal expansion (ZTE) or negative thermal expansion (NTE) are anomalous and indeed rare. Materials with ZTE or NTE are technologically useful in diverse areas such as optics, heat-engine components, structural engineering applications, etc. Characteristic examples of materials that exhibit NTE upon cooling are glasses in the silica−titania family,[1] Ag$_3$[Co(CN)$_6$],[2] metal−organic frameworks,[3] ZrW_2Co_3,[4] anisotropic invar Fe−Ni alloys,[5] certain molecular networks,[6] ruthenium copper oxides,[7] YbGaGe,[8] ytterbium fulleride,[9] and Yb$_8$Ge$_3$Sb$_5$.[10] Sm$_{0.9}$La$_{0.1}$S,[11] CeInCu$_2$,[12] and Ce$_x$La$_{1-x}$Al$_2$[13] show NTE at low temperature (<20 K). In the aforementioned systems, there are a number of physical mechanisms that are known to cause contraction with increasing temperature. These include transverse vibrational modes, rigid-unit modes, phase transitions, and valence fluctuations. Yb exhibits two energetically similar electronic configurations, magnetic Yb^{3+} ($4f^{13}$) and nonmagnetic Yb^{2+} ($4f^{14}$), and as a result can exhibit valence fluctuations, Kondo effects, and heavy-fermion behavior.[14−16] The differing radii of the rare-earth $4f^n$ and $4f^{n-1}$ states can in principle also cause anomalous thermal expansion without an accompanying change in the crystal structure. In the case of YbGaGe, it was shown that the anomalous thermal expansion was due to small-atom interstitial impurities rather than valence fluctuations.[17,18] Here we report that the RE_4TGe$_8$ (RE = Yb, Gd; T = transition metal) family of materials exhibits directional ZTE due to a different process that is associated with the linking of planar square nets in the third dimension.

The new intermetallics Yb$_4T$Ge$_8$ (T = Cr−Ni, Ag) and Gd$_4$CrGe$_8$[19] have the same average structure (Figure 1a) that is related to the CeNiSi$_2$ structure type.[20] The Yb/Gd and Ge atoms occupy the Ce and Si positions, respectively, and T atoms

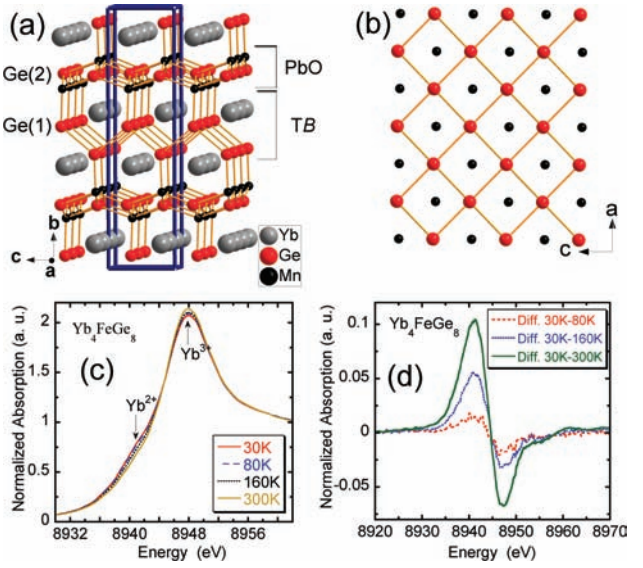

Figure 1. (a) Average structure of Yb$_4T$Ge$_8$ viewed down the a axis. The bonds to the Yb atoms have been omitted to emphasize the 3D [$T_{1/4}$Ge(2)$_2$] framework. The Yb, T, and Ge atoms in Yb$_4T$Ge$_8$ are located in alternating layers stacked along the long b axis in the sequence Yb−T−Ge(2)−T−Yb−Ge(1)−Ge(1)−Yb−T−Ge(2)−T−Yb. The structure can also be described as an intergrowth of distorted PbO- and TB-type layers with the Yb atoms residing within the channels formed by the connection of the two layers. The distorted PbO-type slab contains the T and Ge(2) atoms. The Ge(1) atoms form infinite zigzag chains propagating along the c axis. (b) Square net defined by Ge(2) atoms in the ac plane. The positions of the T atoms alternating above and below this plane are shown. (c) XANES spectra of Yb$_4$FeGe$_8$ sample obtained at various temperatures over the range 15−300 K. The other Yb compounds exhibit similar absorption features. The main absorption peak centered at ∼8948 eV is typical of trivalent Yb in Yb-based intermetallics.[24−26] The spectra also reveal the presence of a weaker feature (shoulder) at 8941−2 eV. This structure, which is ∼7 eV lower in energy relative to Yb^{3+}, is attributed to Yb^{2+} atoms.[24−26] (d) Difference plots (generated by subtracting the data collected at 80, 160, and 300 K from the 30 K data for the Yb$_4$FeGe$_8$ compound) that highlight the enhancement of the Yb^{2+} component.

Received: May 30, 2011
Published: August 04, 2011

adopt the square-pyramidal Ni sites, with the difference being that the T sites are only partially occupied. There are two different sublattices of Ge atoms in the structure: zigzag chains of Ge(1) that propagate along the c axis and square nets consisting of Ge(2) atoms within the ac plane (Figure 1b). The two layers are bridged by the T atoms [via the Ge(1) zigzag chains] along the b axis, forming the three-dimensional (3D) [$T_{1/4}$Ge-$(2)_2$] framework. The connection of the two layers creates channels extending along the c axis (not shown) that accommodate the *RE* atoms.

To probe the Yb valence state in the compounds, we performed X-ray absorption near-edge spectroscopy (XANES) measurements on Yb_4TGe_8 (T = Fe, Cr, Co) at the Yb L_{III}-edge. The absorption spectra for Yb_4FeGe_8 at 30, 80, 160, and 300 K are shown in Figure 1c. Difference plots generated by subtracting the high-temperature data from the data at 30 K are shown in Figure 1d [XANES spectra for other compounds are available in the Supporting Information (SI)]. The XANES spectra show that the relative ratio (Yb^{2+}/Yb^{3+}) of the features at 8941−2 and 8948 eV varies with temperature. Specifically, the low-energy peak originating from the Yb^{2+} ions gradually grows with decreasing temperature, whereas the high-energy peak originating from Yb^{3+} decreases. The intensity increase at 8941−2 eV and concomitant decrease in intensity at 8948 eV imply conversion of Yb^{3+} to Yb^{2+} upon cooling. This behavior establishes that in all three measured compounds the average Yb valence changes continuously with temperature (which is characteristic of intermediate valence materials) and that the Yb^{2+} state has a higher population at lower temperatures. Similar behavior was observed for other intermediate-valence intermetallics such as the $YbCu_{5-x}Ga_x$ series,[21] $YbAl_3$,[22] $YbCu_2Si_2$,[23] and $YbInCu_4$.[24]

Since the XANES experiments indicated a decrease in the average Yb valence upon cooling and Yb^{2+} has a larger ionic radius than Yb^{3+}, we hypothesized that this could potentially counteract the normal lattice contraction upon cooling, leading to a total volume change of zero. To test this hypothesis, we performed temperature-dependent single-crystal X-ray diffraction experiments and determined the unit cell parameters at various temperatures for the Yb_4TGe_8 (T = Cr−Ni) compounds, and indeed, we did observe ZTE in the ac plane. Interestingly, however, as we will show below, this novel effect appears to be related to a geometric mechanism rather than to valence fluctuations.

Figure 2a−e shows the temperature-dependent lengths of the lattice constants a, b, and c for Yb_4TGe_8 (T = Cr−Ni). For all of these compounds, the a and c values remain essentially unchanged over the entire temperature range of 10−300 K. The b value changes only slightly up to ∼100 K and exhibits a more normal linear dependence at higher temperatures. This behavior results in negligible volume expansion from 10 K up to ∼100 K for Yb_4CrGe_8 and Yb_4CoGe_8, 120 K for Yb_4FeGe_8, 150 K for Yb_4MnGe_8, and 160 K for Yb_4NiGe_8. Figure 2f shows the volumes of Yb_4MnGe_8 and Yb_4NiGe_8 as functions of temperature over the range 10−160 K. Above 160 K, the volume shows weak positive thermal expansion (PTE) with a roughly linear response.

What is the driving force for the ZTE of these compounds? Three different factors can be implicated: (a) valence fluctuations of Yb atoms (our original hypothesis), (b) the magnetic/redox instability of the transition metals, and (c) unique features of the structure involving the Ge nets and the structural distortions and interactions thereof. In order to probe these factors,

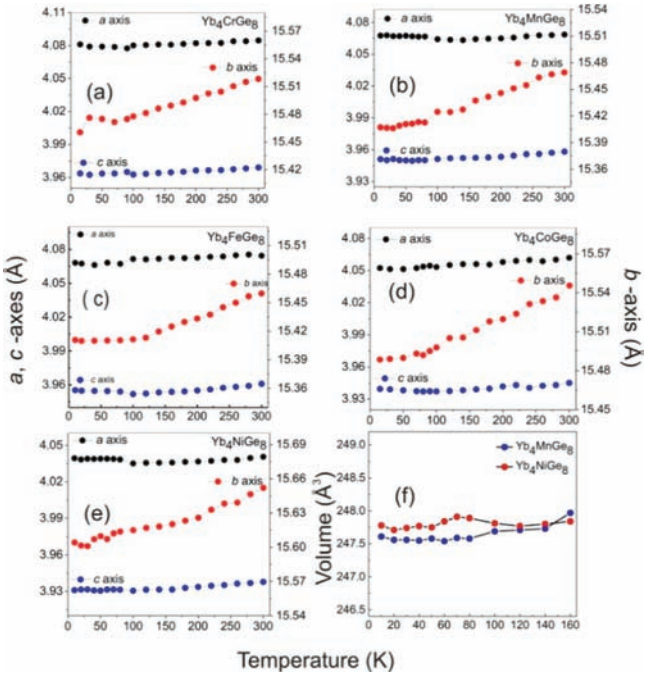

Figure 2. (a−e) Temperature dependence of the unit cell lattice constants a, b, and c for (a) Yb_4CrGe_8, (b)Yb_4MnGe_8, (c) Yb_4FeGe_8, (d) Yb_4CoGe_8, and (e) Yb_4NiGe_8 over the temperature range 10−300 K. The estimated error in these values is 0.001 Å. (f) Temperature dependence of the volumes of Yb_4MnGe_8 and Yb_4NiGe_8 over the range 10−160 K.

we synthesized two control materials: Gd_4CrGe_8 to eliminate the possibility of mixed valency and Yb_4AgGe_8 to eliminate the possible influence of a partially filled d subshell in the transition metal. We observed that the temperature dependence of the lattice constants of Gd_4CrGe_8 and Yb_4AgGe_8 is similarly anomalous, showing ZTE in the Ge square-net plane (ac plane) and very slight expansion perpendicular to it (see the SI). The net result is that the compounds exhibit volume ZTE up to ∼160 K. This rules out the possibility that valence fluctuations in the Yb sublattice and/or the influence of the magnetic transition metal causes the ZTE in Yb_4TGe_8. In addition, the possibility of electron transfer between the T and Ge atoms was ruled out by a detailed temperature-dependent XANES study of Yb_4MnGe_8 at the Mn and Ge edges (see the SI). Consequently, the only features common to all of the compounds are the Ge square nets and the five-coordinate square-pyramidal T metal centers. To understand the Ge square nets, which exhibit long-range modulations, we performed four-dimensional crystallographic refinements.

Supercell Bragg reflections in reciprocal space due to modulation in the structure associated with the Ge square net were indeed observed for RE_4TGe_8 (T = Cr−Fe, Ni). Gd_4CrGe_8 adopts the $Cc(\alpha 0\gamma)s$ superspace group with a $\mathbf{q}$ vector along $^1/_4\mathbf{a}^* + {}^1/_4\mathbf{c}^*$, whereas Yb_4TGe_8 (T = Ag, Co) adopt the $C1(\alpha\beta\gamma)0$ superspace group with a modulation vector along $^1/_4\mathbf{a}^* + {}^1/_4\mathbf{b}^* + {}^1/_4\mathbf{c}^*$ (data collection and structure refinement details are available in the SI).[27] Interestingly, the refinement suggests long-range ordering of the Ge−Ge bonds in the ac plane and also of the T vacancies (Figure 3a−e).

The distortions induced by the occupational modulation of T create a wide distribution of distances between the Ge atoms

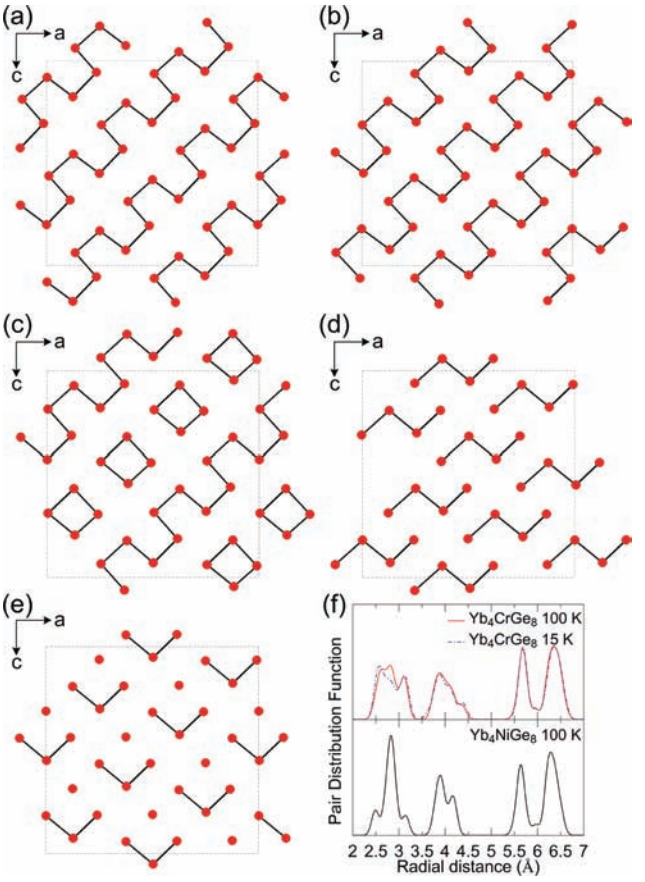

Figure 3. (a–e) Views of the distorted Ge nets at a bonding threshold of 2.8 Å for (a) Yb_4CrGe_8, (b) Yb_4MnGe_8, (c) Yb_4CoGe_8, (d) Yb_4NiGe_8, and (e) Gd_4CrGe_8. (f) PDFs of the interatomic distances of Ge atoms in the nets of Yb_4CrGe_8 at 100 and 15 K (top) and Yb_4NiGe_8 at 100 K (bottom).

within the net. For example, in Yb_4CrGe_8, the minimum and maximum Ge–Ge distances are 2.477(8) and 3.229(8) Å, respectively, at 100 K, and the corresponding values in Yb_4MnGe_8 and Yb_4FeGe_8 are 2.483(9) and 3.225(11) Å and 2.497(9) and 3.262(9) Å, respectively. In Yb_4CoGe_8, however, these values are 2.529(16) and 3.367(18) Å, respectively. In Gd_4CrGe_8, the minimum and maximum Ge–Ge distances are 2.595(8) and 3.192(9) Å, wherease the corresponding distances are 2.488(17) and 3.148(18) Å in Yb_4NiGe_8 and 2.401(11) and 3.299(10) Å in Yb_4AgGe_8. These long-range modulations in the square nets are similar to those observed in charge-density-wave (CDW) compounds.[28]

Figure 3 shows the distorted Ge nets for several of the RE_4TGe_8 compounds using a bonding threshold of ~2.8 Å. Interestingly, the Ge–Ge bonding distribution within the nets differs significantly among the members, as shown by their pair distribution functions (PDFs) (the PDF calculations are described in the SI, and the PDFs for all of the compounds are shown in Figure S4). On the basis of the PDFs, Yb_4CrGe_8 seems to have the greatest number of short Ge–Ge bonds, since the distribution at low distances becomes more intense. This distribution becomes even more asymmetric at lower temperatures (e.g., 15 K; see the dashed blue line in the top panel of Figure 3f), where the population of distances at ~2.75 Å decreases further and migrates to lower radial distances. In a ZTE material, the average interatomic distances remain unchanged as a function of temperature. Consequently, their temperature-dependent PDFs do not show shifts at medium to high radial distances. Indeed, the difference between the PDFs at 100 and 15 K for Yb_4CrGe_8 (Figure 3f top) is negligible at distances >3.5 Å. Interestingly, the Ge–Ge distance distribution in Yb_4NiGe_8, which showed the widest ZTE temperature range, is very different from those of the other compounds at short distances, showing three relatively narrow distributions centered around 2.5, 2.8, and 3.1 Å (Figure 3f bottom).

A common electronic instability in systems with square nets is that of a CDW, where nesting between bands at the Fermi surface leads to a lower broken-symmetry ground state. Therefore, the Fermi surfaces of different models (subcell or supercell with or without vacancies) were calculated using density functional theory (DFT),[29] but none of these topologies gave clear evidence for Fermi surface nesting. The structural modulations arise from the transfer of electron density from the *T* atoms to antibonding orbitals of the Ge net. This charge transfer destabilizes the ideal square-net structure by cleaving an increasing number of Ge–Ge bonds as the d-orbital filling of the *T* atoms increases in moving from left to right across the periodic table.

The anomalous thermal expansion observed in the RE_4TGe_8 compounds is different from the "membrane effect" in layered materials predicted by Lifshitz in 1952.[30] In layered materials with van der Waals gaps and discrete atomic sheets, such as graphite, GeSe, and $TlGaSe_2$, an in-plane NTE effect has been attributed to out-of-plane bending modes.[31,32] These modes are possible because there is no cross-linking of the planes in the perpendicular direction. The modes therefore contribute to large PTE perpendicular to the planes, and these materials do not exhibit ZTE. In the RE_4TGe_8 family, we have a dense 3D structure that does not permit the development of such modes, and therefore, the Lifshitz mechanism cannot apply.

The strong out-of-plane bonds that cross-link the Ge nets through the *T* atoms and the zigzag Ge(1) chains create a flexible 3D framework. As the temperature rises from 0 K, the normal thermal expansion along the *b* axis [perpendicular to the nets of Ge(2) atoms] increases the axial Ge(1)–*T*–Ge(2) bond angles and as a result decreases the basal Ge(2)–*T*–Ge(2) angles. The square-pyramidal coordination of the *T* atom, where the four basal *T*–Ge(2) bonds are oriented toward the net and the axial *T*–Ge(1) bond is perpendicular to it, is a key feature in achieving the ZTE effect shown in Figure 4a,b. As the basal Ge(2)–*T*–Ge(2) angles decrease, there is an overall compression effect in the *ac* plane because of the need to maintain normal *T*–Ge bond lengths (Figure 4c,d). This is a Poisson-like mechanism that acts to squeeze the structure in the *ac* plane. The contracting force is counteracted to a certain extent by the normal thermal expansion with rising temperature, which gives an overall ZTE in the plane. The long-range modulations in the Ge nets are important in allowing this compression because of the long–short alternation of the Ge–Ge bonds, which renders the nets compressible in the *ac* plane.

The RE_4TGe_8 compounds exhibit strongly anomalous thermal expansion properties. Through a series of control experiments, we have ruled out contributions to this behavior from valence fluctuations and magnetic/redox instability. The distorted Ge nets and their ability to adopt varying interatomic bonding distributions at short distances makes them compressible, and this, coupled with the transition-metal-mediated cross-linking in the third dimension, creates a ZTE response in the *ac*

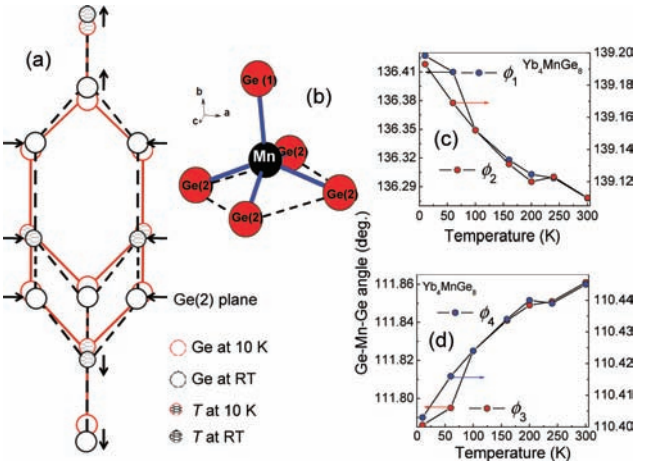

Figure 4. (a) Structural view of temperature-dependent changes in the distances and angles in Yb_4TGe_8. The solid red and dashed black bonds represent the structures at 10 and 300 K, respectively. Arrows indicate the direction of atomic motion with temperature. (b) Five-coordinate square-pyramidal T center with four basal T−Ge(2) bonds and one axial T−Ge(1) bond (shown for T = Mn). (c). Decrease in the Ge(2)−T−Ge(2) angles of the basal bonds (φ_1 and φ_2) with increasing temperature. (d) Increase in the Ge(2)−T−Ge(1) angles of the axial bonds (φ_3 and φ_4) with increasing temperature.

plane. To our knowledge, this is the first time a density-wave type of distortion has been implicated as a reason for anomalous thermal expansion. This insight raises the possibility that such behavior could be sought in materials exhibiting similar structural characteristics and atomic square nets.

■ ASSOCIATED CONTENT

Supporting Information. Details of structural analysis, DFT calculations, crystallographic data, and complete ref 24. This material is available free of charge via the Internet at http://pubs.acs.org.

■ AUTHOR INFORMATION

Corresponding Author
m-kanatzidis@northwestern.edu

■ ACKNOWLEDGMENT

Financial support from the Department of Energy (Grant DE-FG02-07ER46356) is gratefully acknowledged. This work was supported by UChicago Argonne, LLC, which operates Argonne National Laboratory, a U.S. Department of Energy Office of Science laboratory, under Contract DE-AC02-06CH11357. PNC/XOR facilities and research at these facilities are supported by the U.S. DOE.

■ REFERENCES

(1) Schultz, P. C.; Smyth, H. T. In *Amorphous Materials*; Douglas, R. W., Ellis, B., Eds.; Wiley: New York, 1970.
(2) Goodwin, A. L.; Calleja, M.; Conterio, M. J.; Dove, M. T.; Evans, J. S. O.; Keen, D. A.; Peters, L.; Tucker, M. G. *Science* **2008**, *319*, 794.
(3) Han, S. S.; Goddard, W. A., III *J. Phys. Chem. C* **2007**, *111*, 15185.
(4) Mary, T. A.; Evans, J. S. O.; Vogt, T.; Sleight, A. W. *Science* **1996**, *272*, 90.
(5) Shiga, M. *Curr. Opin. Solid State Mater. Sci.* **1996**, *1*, 340.
(6) Baughman, R. H.; Galvao, D. S. *Nature* **1993**, *365*, 735.
(7) Mclaughlin, A. C.; Sher, F.; Attfield, J. P. *Nature* **2005**, *436*, 829.
(8) Salvador, J. R.; Gu, F.; Hogan, T.; Kanatzidis, M. G. *Nature* **2003**, *425*, 702.
(9) Margadonna, S.; Arvanitidis, J.; Papagelis, K.; Prassides, K. *Chem. Mater.* **2005**, *17*, 4474.
(10) Margadonna, S.; Prassides, K.; Chondroudi, M.; Salvador, J. R.; Kanatzidis, M. G. *Chem. Commun.* **2005**, 5754.
(11) Oomi, G.; Kuwahara, R.; Kagayama, T.; Jung, A. *J. Magn. Magn. Mater.* **2001**, *226*, 1182.
(12) Devisser, A.; Bakker, K.; Pierre, J. *Physica B* **1993**, *188*, 577.
(13) Lang, M.; Schefzyk, R.; Steglich, F.; Grewe, N. *J. Magn. Magn. Mater.* **1987**, *63*−*64*, 79.
(14) Alami-Yadri, K.; Wilhelm, H.; Jaccard, D. *Eur. Phys. J. B* **1998**, *6*, 5.
(15) Kowalczyk, A.; Falkowski, M.; Tolinski, T.; Chelkowska, G. *Solid State Commun.* **2006**, *139*, 5.
(16) Jaccard, D.; Link, P.; Vargoz, E.; AlamiYadri, K. *Physica B* **1997**, *230*, 297.
(17) Drymiotis, F. R.; Lee, Y.; Lawes, G.; Lashley, J. C.; Kimura, T.; Shapiro, S. M.; Migliori, A.; Correa, V.; Fisher, R. A. *Phys. Rev. B* **2005**, *71*, 174304.
(18) Booth, C. H.; Christianson, A. D.; Lawrence, J. M.; Pham, L. D.; Lashley, J. C.; Drymiotis, F. R. *Phys. Rev. B* **2007**, *75*, 012301.
(19) (a) Bie, H. Y.; Tkachuk, A. V.; Mar, A. *J. Solid State Chem.* **2009**, *182*, 122. (b) Gil, A.; Kaczorowski, D.; Penc, B.; Hoser, A.; Szytuła, A. *J. Solid State Chem.* **2011**, *184*, 227.
(20) Bodak, O. I.; Gladyshevskii, E. I. *Kristallografiya* **1969**, *14*, 990.
(21) Bauer, E.; Tuan, L.; Hauser, R.; Gratz, E.; Holubar, T.; Hilscher, G.; Michor, H.; Perthold, W.; Godart, C.; Alleno, E.; Hiebl, K. *Phys. Rev. B* **1995**, *52*, 4327.
(22) Lawrence, J. M.; Kwei, G. H.; Canfield, P. C.; Dewitt, J. G.; Lawson, A. C. *Phys. Rev. B* **1994**, *49*, 1627.
(23) Sampathkumaran, E. V.; Gupta, L. C.; Vijayaraghavan, R. *Phys. Lett. A* **1979**, *70*, 356.
(24) Moreschini, L.; et al. *Phys. Rev. B* **2007**, *75*, 35113.
(25) Rao, C. N. R.; Sarma, D. D.; Sarode, P. R.; Sampathkumaran, E. V.; Gupta, L. C.; Vijayaraghavan, R. *Chem. Phys. Lett.* **1980**, *76*, 413.
(26) Hatwar, T. K.; Nayak, R. M.; Padalia, B. D.; Ghatikar, M. N.; Sampathkumaran, E. V.; Gupta, L. C.; Vijayaraghavan, R. *Solid State Commun.* **1980**, *34*, 617.
(27) Further details concerning the crystal structure investigations may be obtained from Fachinformationszentrum Karlsruhe, 76344 Eggenstein-Leopoldshafen, Germany [fax: (+49)7247−808−666; e-mail: crysdata@fiz-karlsruhe.de; Internet: http://www.fiz-karlsruhe.de/request_for_deposited_data.html]. Cambridge Structural Database (CSD) numbers: 422841 (Gd_4CrGe_8 at 100 K), 422842 (Yb_4AgGe_8 at 100 K), 422843 (Yb_4CoGe_8 at 100 K), 422844 (Yb_4CrGe_8 at 15 K), 422845 (Yb_4CrGe_8 at 100 K), 422846 (Yb_4FeGe_8 at 100 K), 422847 (Yb_4MnGe_8 at 100 K), 422848 (Yb_4NiGe_8 at 100 K)
(28) (a) Malliakas, C. D.; Kanatzidis, M. G. *J. Am. Chem. Soc.* **2006**, *128*, 12612. (b) Malliakas, C. D.; Kanatzidis, M. G. *J. Am. Chem. Soc.* **2006**, *128*, 12612. (c) Kim, H. J.; Malliakas, C. D.; Tomić, A. T.; Tessmer, S. H.; Kanatzidis, M. G.; Billinge, S. J. L. *Phys. Rev. Lett.* **2006**, *96*, 226401. (d) Malliakas, C.; Billinge, S. J. L.; Kim, H. J.; Kanatzidis, M. G. *J. Am. Chem. Soc.* **2005**, *127*, 6510.
(29) Results of band structure calculations are available in the SI. The band structures and Fermi surface topologies for Lu_4AgGe_8 models are shown in Figures S5−S10. The atomic coordinates used for the calculations are given in Tables S9−S11.
(30) Lifshits, I. M. *Zh. Eksp. Teor. Fiz.* **1952**, *22*, 475.
(31) Mounet, N.; Marzari, N. *Phys. Rev. B* **2005**, *71*, 205214.
(32) Seyidov, M. Y.; Suleymanov, R. A. *J. Appl. Phys.* **2010**, *108*, No. 063540.